Estimation of Cosinusoidal Displacements using Self-Mixing Interferometry in Moderate Feedback Regime using Deep Learning

Junaid Iqbal Khan
2021317105
Korea Aerosopace University

June 24, 2021

Abstract

In this project, the task of estimating velocity of periodic moving target, as reflected from a recent 2021 paper [2], has not been improved, but the base line deep learning architecture, i.e. 1dCNN has been compared with several other architectures, most of which I have studied in deep learning course. Basically, the work has been aimed towards estimating amplitude and frequency of the vibrating target from self-mixing laser power signals through deep learning, which acts as generalization over just estimating velocity of same targets. Due to lack of any experimental data for deep learning purpose, the signals were simulated through self-mixing equations in MATLAB. The extracted signals were stored in the format of .csv, and then proceeded further on JUPYTER notebook under the umberalla of tensorflow's keras library on python language.

1 Introduction

Optical self-mixing interferometry has been gaining attention recently due to its relatively simple construction [11], as compared to other interferometric schemes, for estimation of displacement.

Basically, what happens in the self-mixing scheme is that we extract a laser power signal from simple laser diode, and estimate displacement from it, utilizing parameters like modulation index (m), linewidth enhancement factor (α) and coupling feedback factor (C). While knowledge of these parameters would induce such measurement scheme somewhat straightforward, in realty such parameters are volatile and might change due to environmental conditions.

Whilst, most research direction upon this has been either towards application direction, e.g.[6, 15] or towards signal processing direction, e.g. [5, 7, 17, 18, 8], the machine learning influence has been pretty sparse in this field and as a matter of fact, has been visible only since 2020 [9, 14, 2]. This lack of machine learning application would very much be of research focus in domain in near future, due to its appealing results.

Therefore, the current project work will bolster my future work in this field and I would surely pursue pushing this current work towards publication.

2 Principle of Self-Mixing Interferometry

Laser light is generated in the optical cavity of a LD and a portion of the laser beam is back-scattered from the remote target and re-enters the active laser cavity. Let $D(t)$ represent the instantaneous distance between the LD driven by a constant injection current and a remote target surface [12]. When this optical feedback phenomenon occurs, the laser wavelength is no longer the constant λ_o but is slightly modified to $\lambda_f(t)$ and varies as $D(t)$ varies. The wavelength fluctuations can be found by solving the well-known excess phase equation based on the Lang and Kobayashi model [10],

$$x_o(t) = x_f(t) + C\sin(x_f(t) + \theta) \tag{1}$$

where $\theta = arctan(\alpha)$ while x_o and x_f are referred to as unperturbed (without feedback) and perturbed (with feedback) phase, respectively, given by,

$$x_o(t) = 2\pi\nu_o(t)\tau(t) \tag{2}$$

$$x_f(t) = 2\pi\nu_f(t)\tau(t) \tag{3}$$

where $\tau(t) = 2D(t)/c$ is the round trip time, with c as speed of light while $\nu_f(t)$ and $\nu_o(t)$ represents optical frequency with and without feedback, respectively.

As C increases from zero, the laser operates into five different regimes [1]. Generally, SM sensing is performed under weak feedback regime ($C < 1$) [16], moderate

Table 1: Tabulation of additional architectures with their compromised parameters, which would be learned on availed dataset

	Architecture	Number of Parameters
1	2 layered MLP	16,002
2	2D CNN	11,854,370
3	AlexNet	62,430,648
4	RNN	1,040,770
5	LSTM	4,162,306
6	GRU	3,122,178
7	4 RNN cells stacked	1,139,458
8	4 LSTM cells stacked	4,557,058
9	4 GRU cells stacked	3,419,394

feedback regime ($1 < C < 4.6$) [4], or strong feedback regime ($C > 4.6$). However, moderate feedback regime is usually preferred over others as the simple saw tooth shaped SM fringes belonging to such a regime intrinsically provide motion direction indication and require simplified SM fringe detection processing (while both tasks are difficult to achieve for weak feedback regime) [3].

Laser diode output optical power, or the so called SM signal, $P(t)$ depends on the SM phenomenon and written as [13],

$$P(t) = P_o[1 + m_i \cos(x_f(t))] \tag{4}$$

where P_o is the power emitted by the free running state LD and m_i is the modulation index. From above, perturbed phase $x_f(t)$ can be extracted, which can be used to calculate unperturbed phase $x_o(t)$ and then $D(t)$ using

$$D(t) = \frac{\lambda_o}{4\pi} x_o(t). \tag{5}$$

3 Methods

For carrying out this project, simulated SM laser power signals and displacements are used, utilizing equations (1), (4) and (5), due to lack of experimentally availed signals due to time and resource constraints. The task of deep learning is directed towards considering standard SM laser signals as input and amplitude-frequency pair as target, as shown in fig.. The reason that target is represented as $\mathbf{R}^2$ is because $[A, f]$ can always be projected to a signal $A\cos(2\pi f t)$, which would be displacement and would be of same dimensions as input. Thus this would reduce the computational complexity associated with deep learning, at least in terms of outermost layer.

Not only this, but also a standard displacement signal can act as a well generalization over velocity [2], such that time derivative of displacement leads to velocity, which would be function of time.

Table 2: Tabulation of additional architectures with their compromised parameters, which would be learned on availed dataset

	Architecture	Training Epochs	Training Accuracy	Validation Accuracy	Predicted Amplitude MSE	Predicted Frequency MSE
1	1dCNN	100	0.97	0.96	86.08nm	431.71mHz
2	Improved 1dCNN	100	0.96	0.99	45.20nm	36.35mHz
3	2 layered MLP	100	0.96	0.87	1405.71nm	969.22mHz
4	2D CNN	300	0.97	0.97	266.37nm	124.66mHz
5	AlexNet	300	0.96	0.97	106.96nm	18.75mHz
6	RNN	100	0.92	0.84	965.90nm	48.23mHz
7	LSTM	100	0.95	0.86	774.92nm	175.41mHz
8	GRU	100	0.94	0.89	612.57nm	38.82mHz
9	4 RNN cells stacked	100	0.91	0.93	991.68nm	434.47mHz
10	4 LSTM cells stacked	100	0.94	0.92	627.66nm	17.73mHz
11	4 GRU cells stacked	100	0.95	0.95	472.53nm	6.50mHz

Moving on, while one dimensional convolutional neural network (1dCNN) was used as the deep learning architecture [2], the project compromises of not only emulation of same architecture (due to its code unavailability), but also it was improved by adding more layers and changing the optimizer. Additionally, several other architectures like CNN, RNN, LSTM and GRU were constructed and tested upon, to permit rigorous comparison of results. All processing carried out in python, tensorflow's keras library was used as the main tool for constructing the architectures.

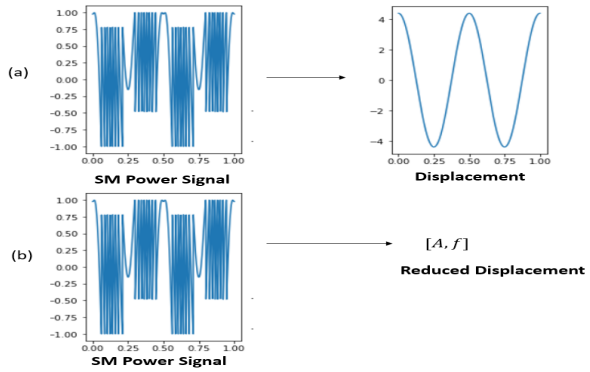

Figure 1: The task of sequence to sequence regression. (a) represents a standard respective setup where input would be SM signal and target should be the corresponding displacement. (b) represents the setup opted in this project where the input being SM signal, the target is the vector of parameters of displacement,i.e. time and frequency

3.1 1dCNN

The architecture of 1dCNN, as described in [2], is shown in fig.1(left). The loss measured in training of the model was based on mean-squared error, and the optimizer opted was 'Adam'. On training and validating the model on 100 epochs, the fig.2 represents the training and validation accuracy and loss.

3.2 Improved 1dCNN

The architecture of improved 1dCNN, as described in [2], is shown in fig.3. It is apparent that with addition of 2 layers, the number of parameters increased by almost 12 folds. Furthermore, the optimizer was replaced by 'RMSprop'. The plot of training and validation accuracy and loss on 100 epochs are shown in fig.4

Layer (type)	Output Shape	Param #
conv1d (Conv1D)	(None, 7994, 16)	128
max_pooling1d (MaxPooling1D)	(None, 3997, 16)	0
conv1d_1 (Conv1D)	(None, 3991, 32)	3616
max_pooling1d_1 (MaxPooling1	(None, 1995, 32)	0
conv1d_2 (Conv1D)	(None, 1989, 64)	14400
max_pooling1d_2 (MaxPooling1	(None, 994, 64)	0
dropout (Dropout)	(None, 994, 64)	0
conv1d_3 (Conv1D)	(None, 988, 64)	28736
max_pooling1d_3 (MaxPooling1	(None, 494, 64)	0
flatten (Flatten)	(None, 31616)	0
dense (Dense)	(None, 16)	505872
dense_1 (Dense)	(None, 2)	34

Total params: 552,786
Trainable params: 552,786
Non-trainable params: 0

Layer (type)	Output Shape	Param #
conv1d (Conv1D)	(None, 7994, 16)	128
max_pooling1d (MaxPooling1D)	(None, 3997, 16)	0
conv1d_1 (Conv1D)	(None, 3991, 32)	3616
max_pooling1d_1 (MaxPooling1	(None, 1995, 32)	0
conv1d_2 (Conv1D)	(None, 1989, 64)	14400
max_pooling1d_2 (MaxPooling1	(None, 994, 64)	0
conv1d_3 (Conv1D)	(None, 988, 128)	57472
max_pooling1d_3 (MaxPooling1	(None, 494, 128)	0
flatten (Flatten)	(None, 63232)	0
dropout (Dropout)	(None, 63232)	0
dense (Dense)	(None, 100)	6323300
dense_1 (Dense)	(None, 50)	5050
dense_2 (Dense)	(None, 2)	102

Total params: 6,404,068
Trainable params: 6,404,068
Non-trainable params: 0

Figure 2: Architechture of 1dCNN (left) and improved 1dCNN (right)

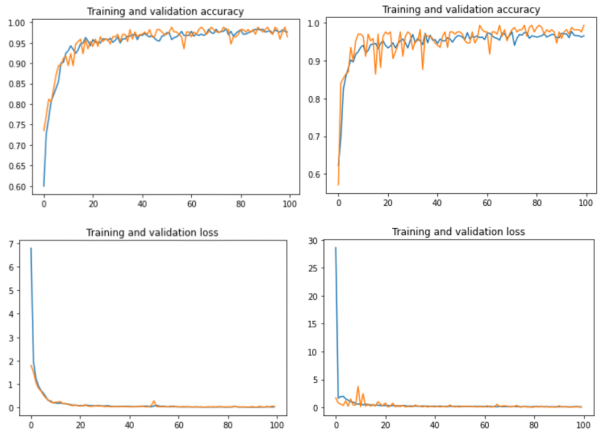

Figure 3: Left figures represent training and validation accuracy and loss history by 1dCNN and right figures represent the same for improved 1dCNN over the dataset, as described in section (3.4)

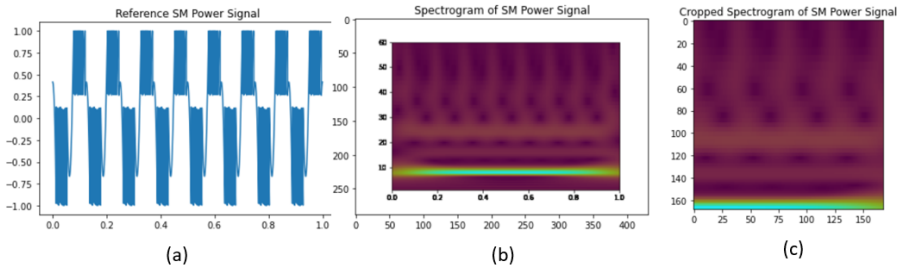

Figure 4: (a) shows sample SM signal (b) shows the corresponding spectrogram (c) shows the cropped spectrogram utilizable for CNN

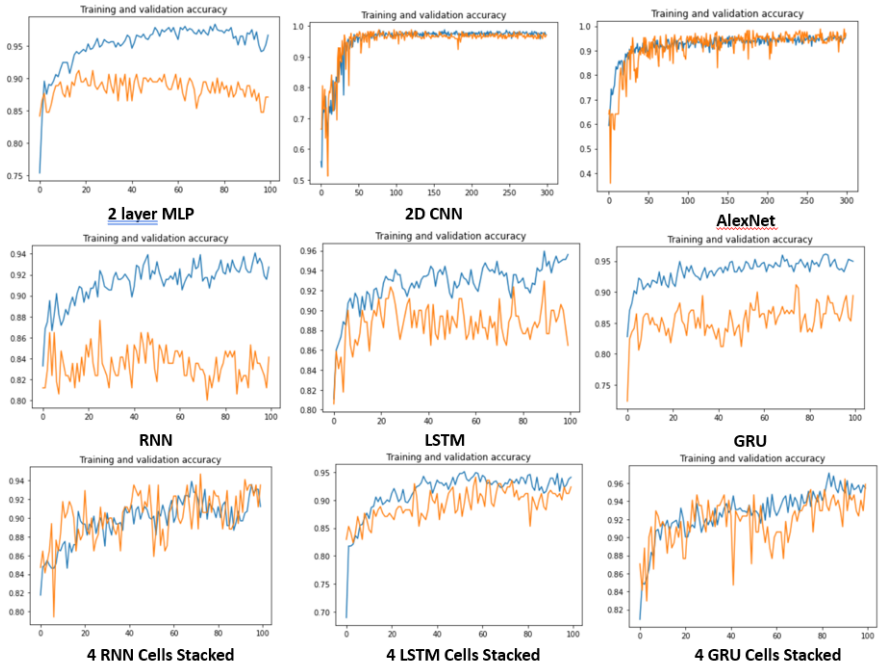

Figure 5: Plots of training and validation accuracy of several architectures proposed in this project (other than 1dCNN and improved 1dCNN) over the described dataset

3.3 Additional Architectures

[2] mentioned of the application of RNN in the context of SM signal to velocity prediction as ”suitable” due to nature of sequence to sequence regression where temporal order matters, but restrained to move in this direction. Their reasoning was that they are hard to train and that application of predicting output is not dependent upon past values.

On the other hand, the shape of SM signal is largely controlled by the optical feedback parameter ’C’, which in real life applications can vary based on interferometer’s physical conditions. Therefore, for real time applications, utilization of architectures like LSTM, RNN or GRU would be prophylactic.

Additionally, it was mentioned of using CNN, but not utilizing 2D CNN was not explained. Although, as far as the author’s experience goes, 2D CNN can be excellent for dealing with 1D signals, once their spectograms are availed. Forexample, given the

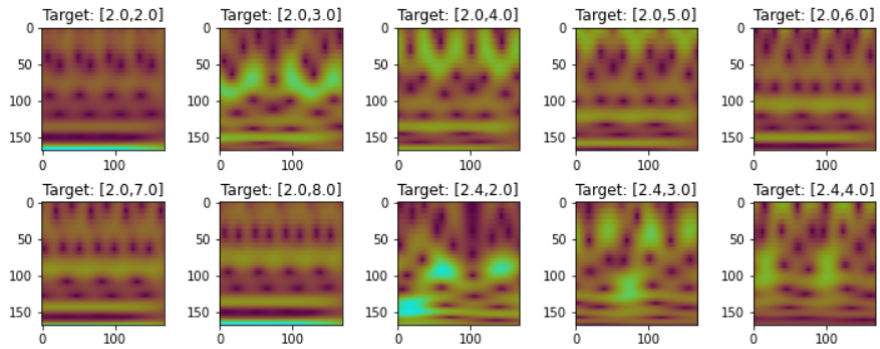

Figure 6: Sample Dataset utilized for 2D CNN architectures, where the title of each image represents output and the image itself is input

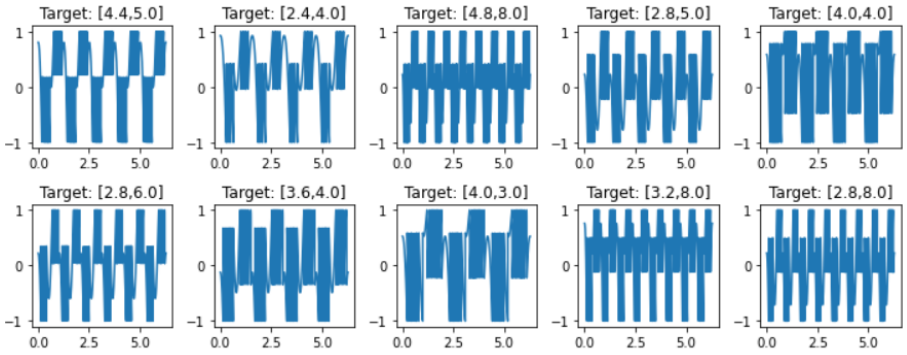

Figure 7: Sample Dataset utilized for non-2D CNN architectures, where the title of each plot image represents output and the signal (of which the plot is shown) is input

sample SM laser power signal, as shown in fig.(4), it's spectrogram, which is the representation of amplitude of frequency content for each time scale, is shown. The way CNN would be beneficial would be to extract features from a detailed representation of signal as a spectrogram, followed by a standard multilayer perceptron setup to make sequent predictions.

To add further resolution towards choice of 1dCNN for carrying out the sequence to sequence regression task, further following architectures were considered and employed:

- **Two layered multilayer perceptron**
- **2D CNN**
- **AlexNet (2D CNN)**
- **RNN**
- **LSTM**
- **GRU**
- **4 RNN cells stacked**

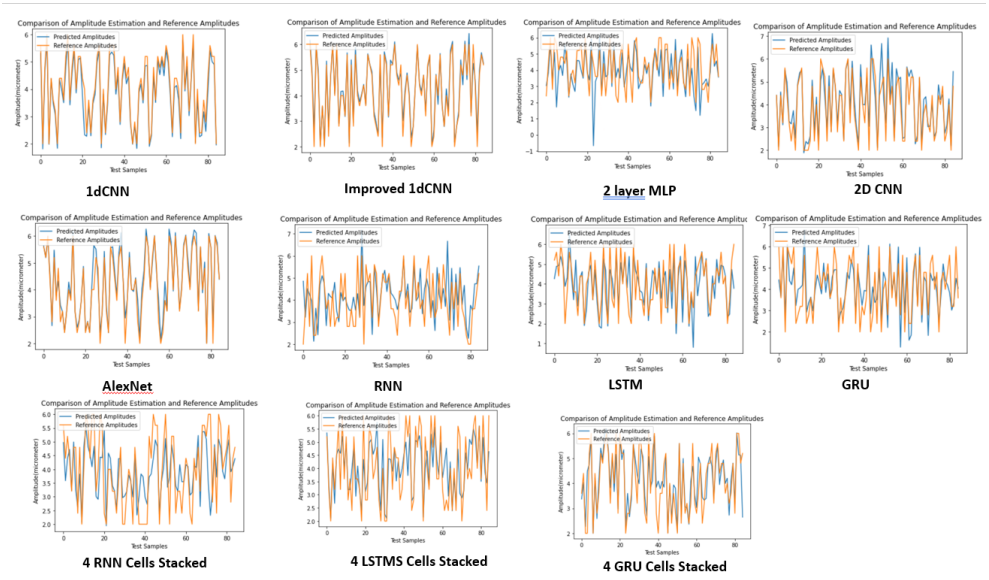

Figure 8: Plot of Reference (orange) and Predicted (blue) Amplitudes from unseen SM Laser Power Signals by several trained architectures proposed in this project

- **4 LSTM cells stacked**
- **4 GRU cells stacked**

The purpose of using 2 layered multilayer perceptron is to have most fundemental deep learner performance reference, upon which all other architectures can be compared with.

3.4 Dataset

The simulated SM signals are extracted by considering the wavelength of light (λ) to be 786nm. The optical feedback parameter C is varied from 2 to 5, amplitude is varied from 2 to 6λ and frequency from 2 to 8Hz.
As described in above subsections, the dataset format for 2D CNN architectures would be spectrogram of SM signals as input and amplitude-frequency pair as target. Sample dataset is shown in fig.(6). Total samples in the dataset are 847 samples.
Likewise, for non-2D CNN architectures, the dataset compromises of SM signals in time domain, as input and amplitude-frequency pair as target. Such sample dataset is shown in fig (7). Total samples in the dataset are 847 samples.

4 Results

After training the mentioned models on datasets, as described in section (3.4), the corresponding results are summarized in table (2). Additionally, to add resolution towards performance of proposed models on unseen data, the comparison plots of reference and predicted amplitudes and frequencies are shown in fig.8 and 9 respectively. Furthermore, the distribution of prediction errors for amplitude and frequency cases are

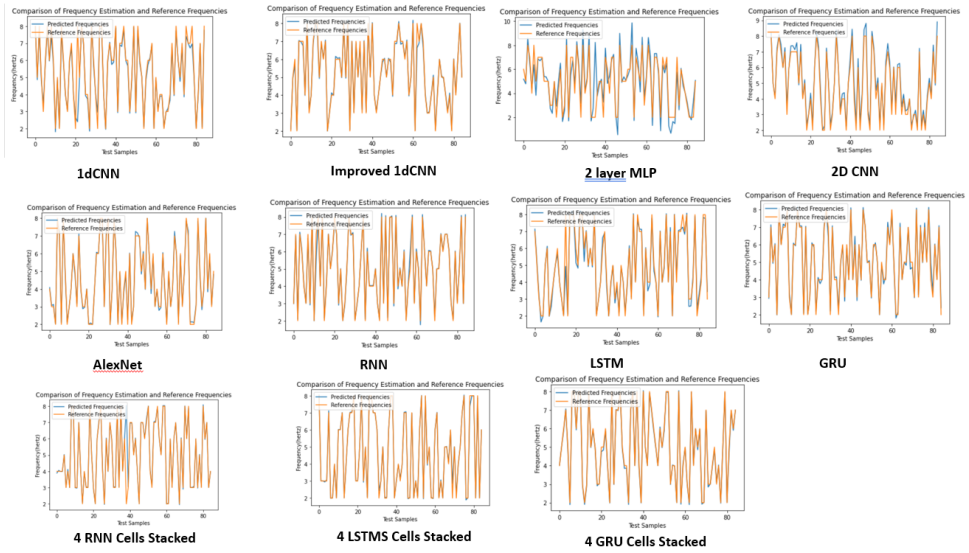

Figure 9: Plot of Reference (orange) and Predicted (blue) Frequencies from unseen SM Laser Power Signals by several trained architectures proposed in this project

provided in fig.10 and 11. Such demonstration of results are not only meant to inform which model works for what attribute prediction, but also inform the nature of the ultimate model which may be most suitable for the contextual sequence to sequence regression.

It is apparent from table (2) that while 1dCNN is the baseline model, whose performance is significant when compared with a simple 2 layered MLP, improved 1dCNN improved the amplitude prediction accuracy by 2 folds and frequency prediction accuracy by 12 folds. Additionally, in terms of just frequency estimation, 4 GRU cells stacked system takes the cake by least frequency estimation error of 6.50mHz. On the other hand, in terms of amplitude estimation, improved 1dCNN is surely the winner.

We can derive a hypothesis that frequency estimation requires long term dependencies between inputs and outputs, while amplitude estimation requires mapping of extract 1D features towards outputs.

The distribution of amplitude estimation errors, as depicted in fig.10, shows that successful models have less standard deviation of their error distribution. While for frequency estimation, it is not the case, but rather spread of error is characteristic of successful model. Therefore, amplitude and frequency mapping from SM signals are intrinsically two very different problems.

5 Conclusions

The purpose of this project was to not only construct and improve the baseline model, as proposed in [2], but also generalize the instilled context of sequence to sequence regression towards a more general scenario. Additionally, to add further resolution towards how deep learning models interact with the given problem of determining displacement from SM laser power signals, many other related models, mentioned in [2]

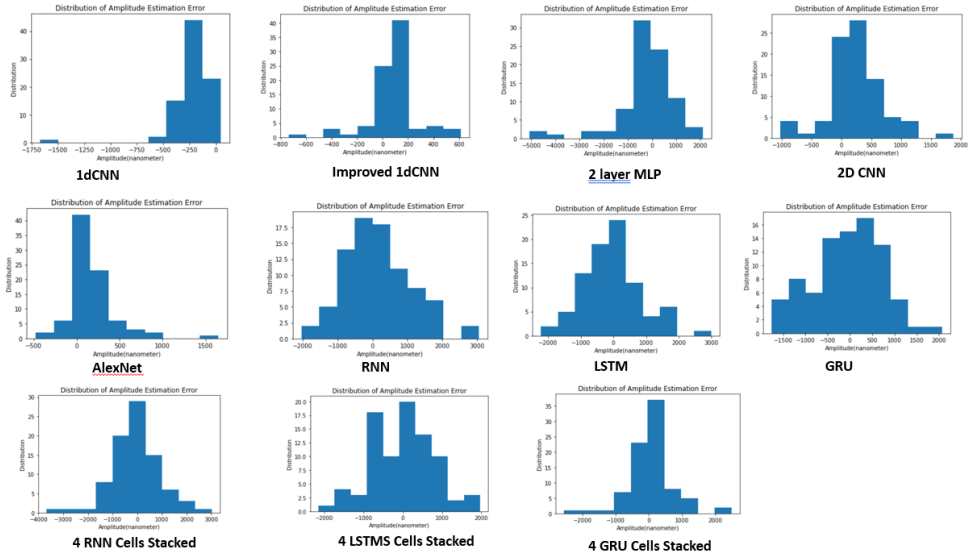

Figure 10: Histogram plot of distributions of amplitude estimation error by several trained architectures proposed in this project

(but not tested), were tested upon to provide insight into what does mapping of SM signals towards displacement parameters require, as discussed in section (4).

References

[1] G. Acket, D. Lenstra, A. Den Boef, and B. Verbeek. The influence of feedback intensity on longitudinal mode properties and optical noise in index-guided semiconductor lasers. *IEEE Journal of Quantum Electronics*, 20(10):1163–1169, 1984.

[2] S. Barland and F. Gustave. Convolutional neural network for self-mixing interferometric displacement sensing. *Optics Express*, 29(8):11433–11444, 2021.

[3] O. D. Bernal, H. C. Seat, U. Zabit, F. Surre, and T. Bosch. Robust detection of non-regular interferometric fringes from a self-mixing displacement sensor using bi-wavelet transform. *IEEE Sensors Journal*, 16(22):7903–7910, 2016.

[4] C. Bes, G. Plantier, and T. Bosch. Displacement measurements using a self-mixing laser diode under moderate feedback. *IEEE transactions on instrumentation and measurement*, 55(4):1101–1105, 2006.

[5] V. Contreras, J. Lonnqvist, and J. Toivonen. Edge filter enhanced self-mixing interferometry. *Optics letters*, 40(12):2814–2817, 2015.

[6] S. Donati and M. Norgia. Self-mixing interferometry for biomedical signals sensing. *IEEE Journal of selected topics in quantum electronics*, 20(2):104–111, 2013.

[7] Y. Gao, Y. Yu, J. Xi, Q. Guo, J. Tong, and S. Tong. Improved method for estimation of multiple parameters in self-mixing interferometry. *Applied optics*, 54(10):2703–2709, 2015.

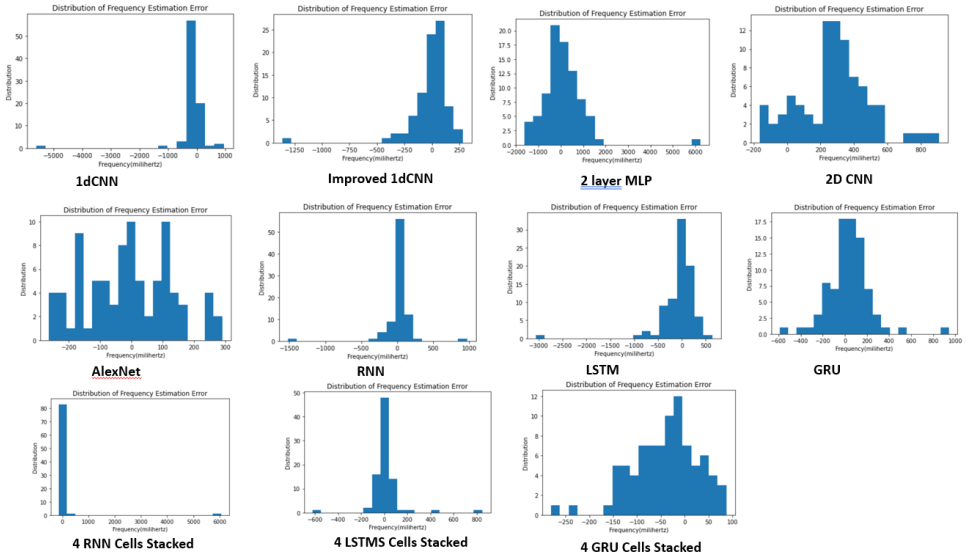

Figure 11: Histogram plot of distributions of frequency estimation error by several trained architectures proposed in this project

[8] J.-H. Kim, C.-H. Kim, T.-H. Yun, H.-S. Hong, K.-M. Ho, and K.-H. Kim. Joint estimation of self-mixing interferometry parameters and displacement reconstruction based on local normalization. *Applied Optics*, 60(8):2282–2287, 2021.

[9] K. Kou, C. Wang, T. Lian, and J. Weng. Fringe slope discrimination in laser self-mixing interferometry using artificial neural network. *Optics & Laser Technology*, 132:106499, 2020.

[10] R. Lang and K. Kobayashi. External optical feedback effects on semiconductor injection laser properties. *IEEE journal of Quantum Electronics*, 16(3):347–355, 1980.

[11] M. Norgia and S. Donati. A displacement-measuring instrument utilizing self-mixing interferometry. *IEEE Transactions on instrumentation and measurement*, 52(6):1765–1770, 2003.

[12] G. Plantier, C. Bes, and T. Bosch. Behavioral model of a self-mixing laser diode sensor. *IEEE Journal of Quantum Electronics*, 41(9):1157–1167, 2005.

[13] T. Taimre, M. Nikolić, K. Bertling, Y. L. Lim, T. Bosch, and A. D. Rakić. Laser feedback interferometry: a tutorial on the self-mixing effect for coherent sensing. *Advances in Optics and Photonics*, 7(3):570–631, 2015.

[14] M. Usman, U. Zabit, and S. A. Alam. Classification of laser modality for a self-mixing interferometric sensor. *Applied Optics*, 59(36):11351–11358, 2020.

[15] X.-l. Wang, L.-p. Lü, L. Hu, and W.-c. Huang. Real-time human blood pressure measurement based on laser self-mixing interferometry with extreme learning machine. *Optoelectronics Letters*, 16(6):467–470, 2020.

[16] J. Xi, Y. Yu, J. F. Chicharo, and T. Bosch. Estimating the parameters of semiconductor lasers based on weak optical feedback self-mixing interferometry. *IEEE Journal of Quantum Electronics*, 41(8):1058–1064, 2005.

[17] Y. Yang and X. Li. Self-mixing interferometry based on improved all-phase fft for high-precision displacement measurement. In *2019 12th International Congress on Image and Signal Processing, BioMedical Engineering and Informatics (CISP-BMEI)*, pages 1–5. IEEE, 2019.

[18] Z. Zhang, C. Li, and Z. Huang. Vibration measurement based on multiple hilbert transform for self-mixing interferometry. *Optics Communications*, 436:192–196, 2019.